Check for updates

Angewandte Chemie International Edition

Angewandte International Edition Chemie

How to cite: *Angew. Chem. Int. Ed.* **2026**, e7491177
doi.org/10.1002/anie.7491177

RESEARCH ARTICLE OPEN ACCESS

Phenonium-Ion-Mediated Skeletal Editing of Paracyclophanes

Tilman Köhler[1] | Pascal Marx[1] | André Jung[2] | Maximilian Hartmann[3] | Jasmin Seibert[1] | Olaf Fuhr[4] | Eli Zysman-Colman[2] | Stefan Bräse[1,3]

[1]Institute of Organic Chemistry (IOC), Karlsruhe Institute of Technology (KIT), Karlsruhe, Germany | [2]Organic Semiconductor Centre, EaStCHEM School of Chemistry, University of St Andrews North Haugh, St Andrews, Fife, UK | [3]Institute of Biological and Chemical Systems – Functional Molecular Systems (IBCS-FMS), Karlsruhe Institute of Technology (KIT), Karlsruhe, Germany | [4]Institute of Nanotechnology (INT) and Karlsruhe Nano Micro Facility (KNMFi), Karlsruhe Institute of Technology (KIT), Karlsruhe, Germany

Correspondence: Stefan Bräse (braese@kit.edu)

Received: 20 August 2026 | **Revised:** 7 October 2026 | **Accepted:** 10 October 2026

Keywords: chemistry | density functional theory | halide | nuclear magnetic resonance spectroscopy | nucleophile | regioselectivity

ABSTRACT

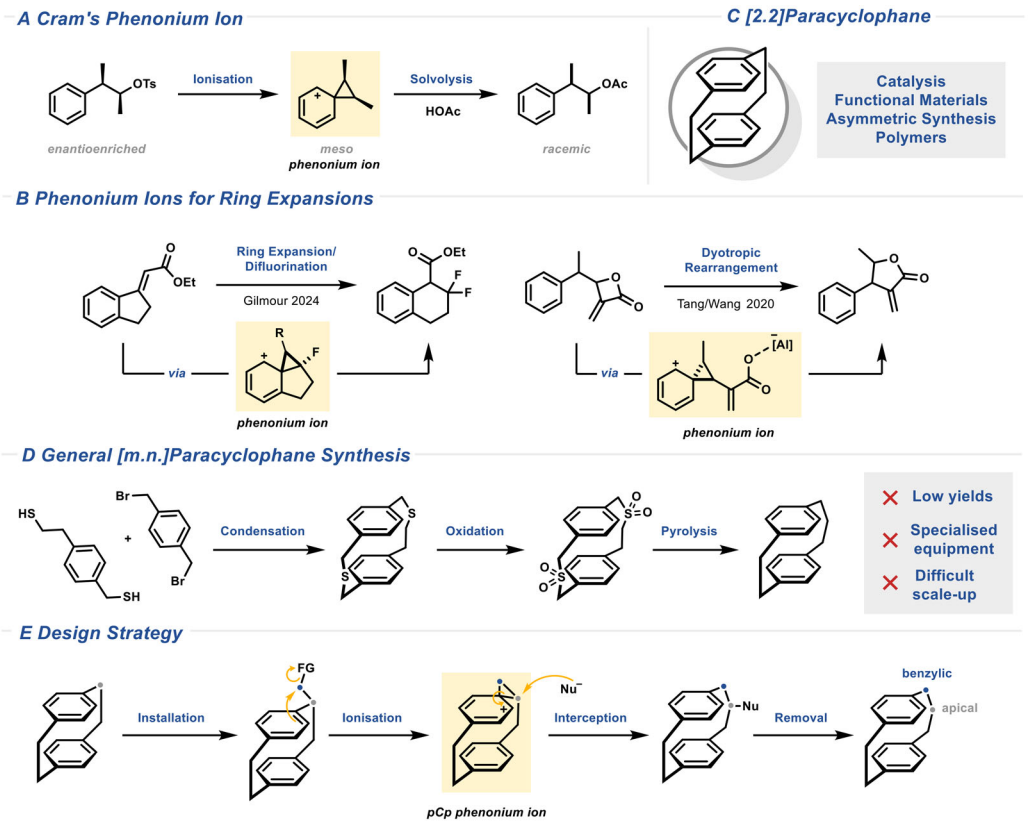
Phenonium ions have played a central role in physical–organic chemistry, yet their use as strategic intermediates in synthesis remains underexplored. Here, we report a phenonium-ion-mediated strategy for the skeletal editing of paracyclophanes. Installation of a one-carbon handle at the aliphatic bridge, followed by direct alcohol activation with $BF_3{\cdot}OEt_2$ under solvolysis-avoiding conditions, generates a paracyclophane-derived phenonium ion that undergoes regioselective ring opening by external nucleophiles. This strategy provides modular access to functionalized higher paracyclophane homologues and tolerates S-, N-, C-, selenium-, and halide-based nucleophiles under operationally simple, gram-scalable conditions. The sequence can be applied iteratively and extended to double bridge expansion, while reductive desulfurization furnishes the corresponding parent hydrocarbons. Mechanistic studies combining nuclear magnetic resonance spectroscopy, kinetic analysis, stereochemical probes, and density functional theory calculations support a self-accelerating mechanism in which product water shifts BF_3 speciation toward $BF_3{\cdot}H_2O$, which assists leaving-group departure through hydrogen-bond donation and thereby facilitates phenonium-ion formation. Together, these results establish paracyclophane-derived phenonium ions as controllable intermediates for skeletal editing and provide practical access to higher paracyclophane topologies with application potential in functional materials, as exemplified by a bridge-expanded thermally activated delayed fluorescence (TADF) emitter.

1 | Introduction

Phenonium ions occupy a distinctive place in carbocation chemistry. First invoked by Cram in 1949 to rationalize the stereochemical outcome of solvolytic Wagner–Meerwein rearrangements through aryl anchimeric assistance, phenonium ions soon became closely intertwined with the classical/nonclassical carbocation debate (Scheme 1A) [1–3]. ^{13}C nuclear magnetic resonance (NMR) studies by Olah in 1971 ultimately settled this question, establishing phenonium ions as classical, spirocyclic carbocations [4–7]. However, despite their prominent role in physical–organic chemistry, phenonium ions have only gradually been harnessed as strategic intermediates in organic synthesis [8].

From a synthetic perspective, the central challenge is taming the high intrinsic reactivity of these cationic species. Early studies largely relied on activated substrates featuring good leaving groups and electron-rich aryl systems. More recent advances, including hexafluoroisopropanol (HFIP)-enabled ionization of 2-arylethanols, reagent-controlled regioselective open-

This is an open access article under the terms of the Creative Commons Attribution License, which permits use, distribution and reproduction in any medium, provided the original work is properly cited.
© 2026 The Author(s). *Angewandte Chemie International Edition* published by Wiley-VCH GmbH



SCHEME 1 | (A) Phenonium ion in Cram's seminal solvolysis studies. (B) Recent examples of phenonium-ion-mediated ring expansion. (C) Representative applications of the [2.2]paracyclophane scaffold. (D) Conventional access to higher paracyclophanes via dithiacyclophanes and sulfur extrusion. (E) This work: strategic use of paracyclophane-derived phenonium ions for skeletal editing.

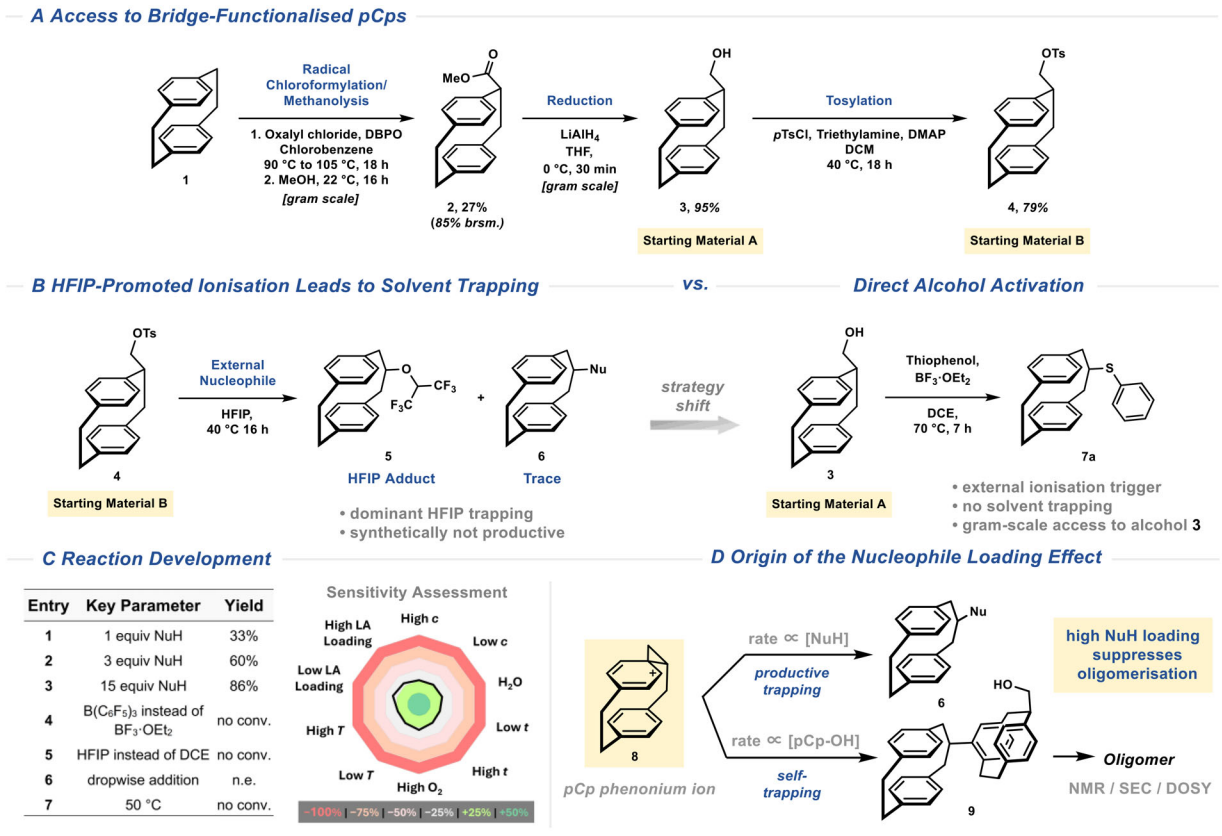
ing of unsymmetrical phenonium ions, and hypernucleofuge-based strategies using hypervalent iodine reagents, have broadened the substrate scope of phenonium-ion chemistry and enabled increasing control over both cation formation and interception through judicious reaction design [9–15]. Importantly, studies from the groups of Gilmour and Tang/Wang have shown that phenonium ions can be used as synthetic tools for the ring expansion of cyclic scaffolds (Scheme 1B) [16, 17]. Beyond these isolated examples, however, the use of phenonium ions as a design principle for skeletal editing remains underappreciated. Herein, this concept is translated to the skeletal editing of paracyclophanes, using paracyclophane-derived phenonium ions to modularly access higher cyclophane homologues.

Paracyclophanes (pCps) are strained hydrocarbon scaffolds in which two co-facially stacked aromatic decks are held in close proximity by aliphatic bridges. Among them, [2.2]paracyclophanes are the most widely studied representatives, with two ethylene bridges locking the aromatic decks into a rigid, distorted arrangement (Scheme 1C). This constrained geometry promotes through-space π-interactions between the decks and, upon suitable substitution, can give rise to planar chirality. Together, these features have made [2.2]pCps valuable motifs in catalysis, asymmetric synthesis, polymer chemistry, and functional materials [18–23].

Although arene-deck functionalization has enabled broad diversification of the [2.2]pCp scaffold, methods for modifying the ethylene bridges remain far less advanced [24–28]. Still more limited are approaches that edit the bridge architecture itself, despite the fact that bridge length directly controls strain, interdeck distance, molecular geometry, and transannular electronic communication. The ability to modulate these parameters would therefore be highly attractive for diverse applications, yet the synthetic access needed to explore higher and unsymmetrically bridged pCp homologues in this context is severely restricted [29, 30]. Today, access to the latter mainly relies on high-dilution condensation to form dithia- or sulfone-bridged cyclophanes, followed by extrusion of sulfur (photochemically) or SO_2 (via flash-vacuum pyrolysis) (Scheme 1D). These routes are limited by the low-yielding condensation step and by the practical constraints of specialised equipment, which precludes routine use and complicates scale-up [29, 31, 32]. Consequently, operationally simple, scalable, and modular strategies for homologating readily available [2.2]paracyclophanes into higher cyclophane frameworks are still needed, making pCps an attractive but challenging target class for skeletal editing [33]. Prior studies of pCp-derived phenonium ions, however, were conducted in the context of solvolysis experiments, where solvent capture of the cationic intermediate offered little opportunity for synthetic diversification [34–37]. We sought to develop a strategy that would suppress solvent trapping and redirect the pCp-derived phenonium ion toward selective interception by external nucleophiles.

The presented strategy relies on the selective installation of a one-carbon handle at the ethylene bridge of [2.2]paracyclo-

15213773, 0, Downloaded from https://onlinelibrary.wiley.com/doi/10.1002/anie.74911177 by Karlsruher Institut Fur Technologie, Wiley Online Library on [10/11/2026]. See the Terms and Conditions (https://onlinelibrary.wiley.com/terms-and-conditions) on Wiley Online Library for rules of use; OA articles are governed by the applicable Creative Commons License



SCHEME 2 | (A) Synthesis of bridge-functionalised [2.2]paracyclophane precursors. (B) Strategic shift from tosylate ionization in HFIP to direct alcohol activation to avoid solvolysis. (C) Reaction development and sensitivity assessment; isolated yields are given. Common conditions: pCp alcohol **3** (0.50 mmol, 1.0 equiv.), $BF_3{\cdot}OEt_2$ (1.0 equiv.), DCE (0.25 M), 70°C, 7 h. NuH = thiophenol; nucleophile loading and other deviations from these conditions are specified in the table. Abbreviations: LA = Lewis acid, DCE = 1,2-dichloroethane, brsm = based on recovered starting material, c = concentration, t = reaction time, T = temperature, H_2O = added water, and O_2 = oxygen. (D) Self-trapping of the pCp phenonium ion accounts for the nucleophile-loading effect.

phane, followed by phenonium ion formation and nucleophilic interception to achieve the desired ring expansion (Scheme 1E). Overall, the introduced carbon atom is rearranged into the cyclophane bridge and occupies the benzylic position, whereas the nucleophile that traps the cation becomes attached at the apical position of the expanded bridge. Subsequent removal of the functional handle can furnish the corresponding cyclophane homologue. Realizing this design therefore required identifying conditions that would convert a historically difficult-to-control cationic intermediate into a synthetic tool for skeletal editing.

2 | Results and Discussion

The required bridge functionality was introduced by radical chloroformylation of [2.2]paracyclophane (**1**) [38, 39] followed by reduction of the resulting pCp ester **2** to the alcohol **3** (Starting Material A), which was subsequently transformed to the corresponding pCp tosylate **4** (Starting Material B) (Scheme 2A).

Conceptually guided by recent reports on HFIP-based phenonium-ion chemistry [15], we first examined whether the corresponding pCp tosylate **4** (Starting Material B) could be ionized in HFIP (Scheme 2B). Indeed, ionization was observed under these conditions; however, the resulting pCp-derived phenonium ion was rapidly intercepted by the weakly nucleophilic solvent, delivering the HFIP adduct **5** as the major product (see Section S3.6). This outcome highlighted the need to generate the phenonium intermediate while avoiding solvent trapping and enabling interception by an external nucleophile. We therefore turned to direct activation of pCp alcohol **3** (Starting Material A) under nonpolar conditions. This precursor is readily available in two steps on multigram scale and allows the ionization to be triggered by an external Lewis or Brønsted acid. Using 1,2-dichloroethane (DCE) as solvent and thiophenol as a model nucleophile, we evaluated a broad set of acids. Most candidates either failed to activate the starting material or led to unproductive pathways (see Section S3.7). $BF_3{\cdot}OEt_2$ was uniquely effective, giving full conversion and the rearranged [3.2]paracyclophane thioether **7a** in an initial 33% yield. Other boron Lewis acids, such as $B(C_6F_5)_3$, did not promote the transformation under otherwise identical conditions (Scheme 2C, entry 4). Although phenonium-ion generation from alcohols has literature precedent under HFIP/TfOH or superacidic conditions, such reactivity under nonpolar conditions has, to the best of our knowledge, not been reported [15, 40].

Reaction optimization identified nucleophile loading as the key parameter: with the model nucleophile, the yield increased from

15213773, 0, Downloaded from https://onlinelibrary.wiley.com/doi/10.1002/anie.7491177 by Karlsruher Institut Fur Technologie, Wiley Online Library on [10/11/2026]. See the Terms and Conditions (https://onlinelibrary.wiley.com/terms-and-conditions) on Wiley Online Library for rules of use; OA articles are governed by the applicable Creative Commons License

33% with 1 equivalent (Scheme 2C, entry 1) to 60% with 3 equivalents (entry 2) and 86% with 15 equivalents (entry 3). No conversion was observed at 50°C (entry 7). HFIP alone was ineffective, and combining HFIP with $BF_3{\cdot}OEt_2$ also led to no conversion, presumably because the Lewis acid is sequestered by the alcohol solvent (entry 5). A Glorius-type sensitivity assessment [41] showed that the transformation tolerates air and small deviations in concentration or temperature, while prolonged reaction times of up to 40 h did not erode the yield, indicating that the thioether product is stable under the reaction conditions. In contrast, both lower and higher Lewis acid loadings had a negative effect on the outcome. Unexpectedly for a transformation initiated by $BF_3{\cdot}OEt_2$, the reaction also proved somewhat tolerant to water, an observation that would later become central to the mechanistic analysis (see Section S3.8).

We next examined why the reaction depends so strongly on nucleophile loading (Scheme 2D). When only one equivalent of thiophenol was used, an additional side-product fraction was isolated alongside the desired [3.2]pCp thioether **7a**. This material was not detected under the optimized conditions, indicating that it arises from a competing pathway that becomes relevant at low nucleophile concentration. NMR spectroscopy, including diffusion-ordered spectroscopy (DOSY), together with size-exclusion chromatography (SEC) analysis showed that this material is not a discrete compound but a pCp-derived oligomeric mixture. A related material was also formed in the absence of an external nucleophile. We therefore attribute this competing pathway to repeated Friedel–Crafts-type self-trapping of phenonium ion **8** by the starting pCp alcohol **3**. Thus, although lower nucleophile loadings still afforded synthetically useful yields, the use of a large excess of nucleophile can be mechanistically rationalized by the need to efficiently outcompete self-trapping. Following this rationale, we examined whether slow addition of pCp alcohol **3**, intended to maintain a low substrate concentration and thereby suppress oligomerization, would improve the yield (Scheme 2C, entry 6). However, this modification had no beneficial effect (see Section S3.9).

Based on these results, we defined two sets of conditions. Thiol nucleophiles were used in 15 equivalents to maximize yield, since the excess reagent could be readily removed by a basic aqueous wash. Non-thiol nucleophiles were used in three equivalents as a compromise between yield and ease of purification. In both cases, the reaction was performed with 1.0 equivalent of $BF_3{\cdot}OEt_2$ in DCE at 70°C and required neither dry solvent nor an inert atmosphere, making the setup operationally straightforward.

With an optimized protocol in hand, we investigated the range of nucleophiles capable of intercepting the pCp-derived phenonium ion under these conditions (Scheme 3). Aryl thiols bearing electron-donating and electron-neutral substituents all afforded the corresponding [3.2]paracyclophane thioethers in high yields, ranging from 71% to 86%, with electron-poor 4-nitrobenzenethiol furnishing **7g** in 60% yield. Substitution at the aryl thiol was also well tolerated, including ortho-substitution (**7i**, 76%) and extended aromatic systems (**7h**, 70%). The reaction further accommodated benzylic (**7k**, 88%), linear aliphatic (**7l**, 53%), branched aliphatic (**7m**, 69%), and cyclic (**7n**, 80%; **7o**, 63%) thiols, giving the corresponding thioethers in moderate to high yields.

The scope of non-thiol nucleophiles was then evaluated using the three-equivalent protocol as described above. Under these more demanding conditions, nitrogen-based trapping proceeded through a Ritter-type manifold with aryl nitriles **Nu10a–Nu10d** to furnish the corresponding amide products (**10a–10d**, 46% to 64%). Alkyl nitriles were generally not tolerated, presumably because they sequestered the Lewis acid more efficiently than aryl nitriles. A notable exception was pivalonitrile (**Nu10e**), which delivered the corresponding amide **10e** only when the $BF_3{\cdot}OEt_2$ loading was increased to three equivalents in a yield of 22%.

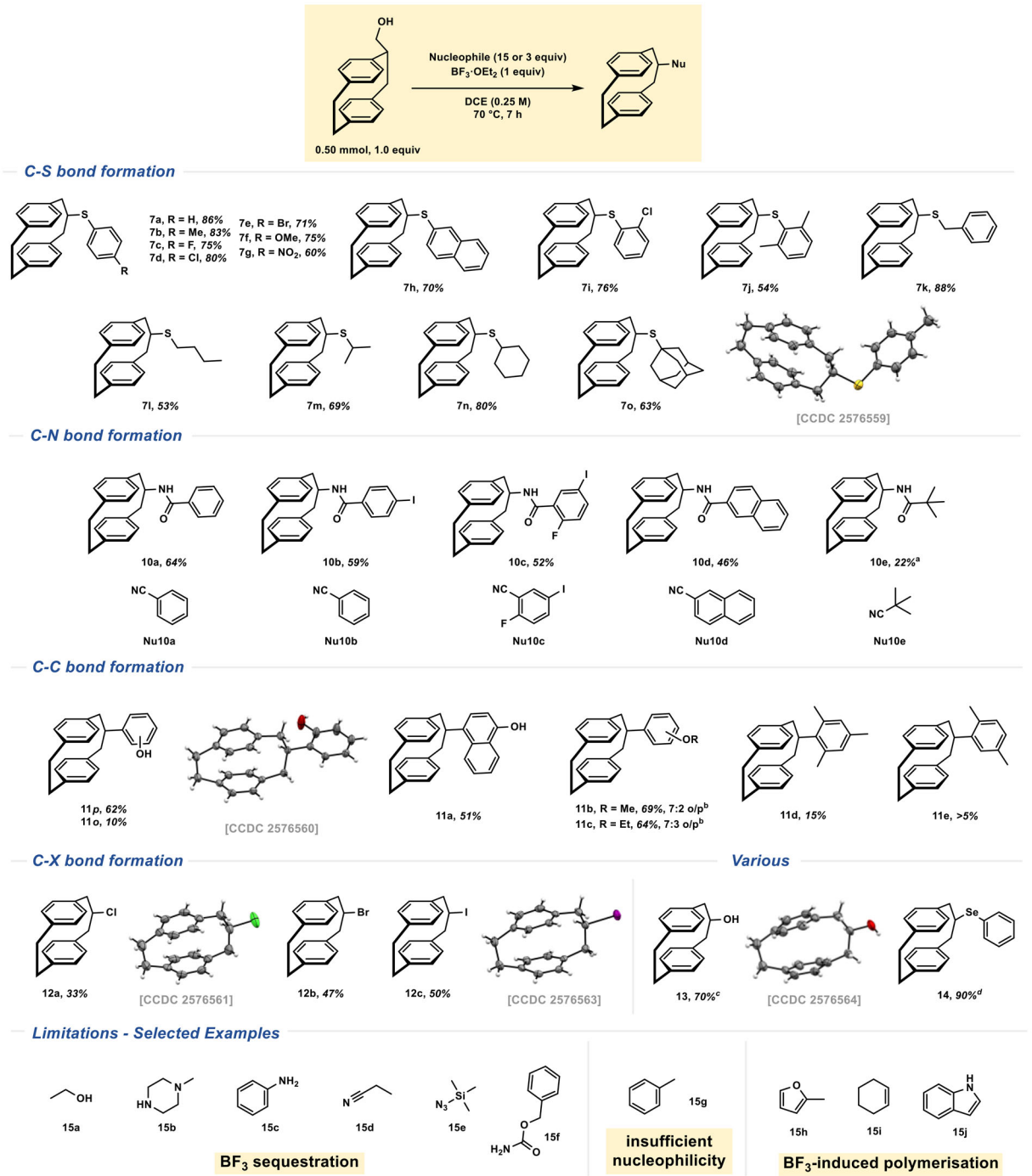
Carbon-based trapping was possible but showed a clear dependence on the nucleophilicity of the arene partner. Phenolic nucleophiles reacted via C—C rather than C—O bond formation, likely because coordination of the phenolic oxygen to $BF_3{\cdot}OEt_2$ deactivates the oxygen center (**11a**, 51%; **11*o*/*p***, 72% combined yield). Electron-rich anisole (**11b**, 69%) and phenetole (**11c**, 64%) intercepted the cationic intermediate in moderate yields, whereas the less nucleophilic mesitylene gave the corresponding product **11d** in a substantially lower 15% yield. The behavior of 1,4-xylene was particularly informative: it provided only trace amounts of the trapping product **11e** alongside the oligomeric side product, whereas less electron-rich toluene led exclusively to oligomerization. These observations suggest that xylene lies near the electronic threshold required for external arene trapping to compete with self-trapping by the pCp alcohol **3**.

Halide incorporation was achieved using trimethylsilyl (TMS) halide sources, providing access to the corresponding chloro-, bromo-, and iodo-substituted [3.2]paracyclophanes (**12a–12c**, 33–50%). Allyltrimethylsilane (allyl-TMS) showed distinct reactivity. Instead of furnishing the allylated [3.2]pCp product, the reaction initially provided a mixture of the starting [2.2]pCp alcohol **3** and the rearranged [3.2]pCp alcohol **13**. Extending the reaction time to 36 h led to full conversion and afforded the [3.2]pCp alcohol **13** in 70% yield. In contrast, the use of only one equivalent of allyl-TMS resulted in oligomerization. Although the exact role of allyl-TMS in this process remains unclear, these observations suggest that it acts as a reaction additive, enabling interception of the phenonium ion by the oxygen atom of the leaving group generated upon ionisation (see Section S3.10). Notably, selenoether **14** was obtained in 90% yield using reduced loading of 5 equivalents of benzeneselenol, highlighting the high trapping efficiency of this softer nucleophile.

Importantly, downstream functionalisation of the apical bridge position in [3.2]paracyclophane derivatives is severely limited, since classical S_N2 displacement is precluded by the inaccessible backside trajectory. This limitation underscores the value of introducing different nucleophiles during the phenonium-ion-mediated rearrangement itself, since it provides direct access to products that cannot be obtained by simple post-functionalisation of, for example, [3.2]paracyclophane iodide **12c**.

The limitations uncovered during our studies fall into three categories: (1) strongly Lewis-basic nucleophiles (e.g. amines, alcohols, anilines), which sequester $BF_3{\cdot}OEt_2$ and thereby prevent ionization altogether; (2) weakly nucleophilic arenes, which do not interfere with ionization but fail to outcompete self-trapping once the pCp phenonium ion has formed (e.g. toluene);

15213773, 0, Downloaded from https://onlinelibrary.wiley.com/doi/10.1002/anie.74911?7 by Karlsruher Institut Fur Technologie, Wiley Online Library on [10/11/2026]. See the Terms and Conditions (https://onlinelibrary.wiley.com/terms-and-conditions) on Wiley Online Library for rules of use; OA articles are governed by the applicable Creative Commons License

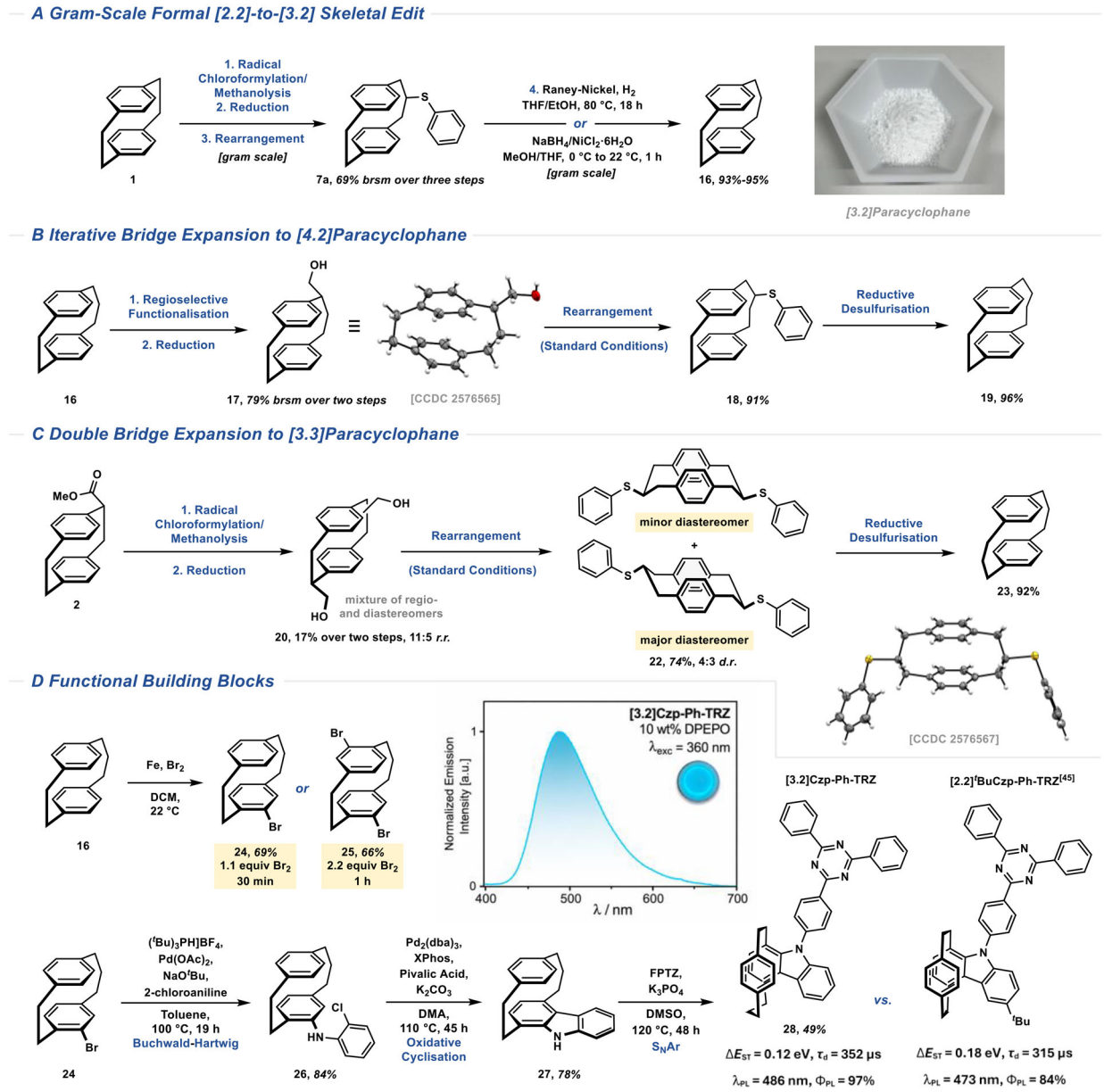


SCHEME 3 | Nucleophile scope investigation. General reaction conditions are shown in the scheme. Isolated yields are given. [a]3.00 equiv. of $BF_3{\cdot}OEt_2$ were used. [b]The combined yield of both regioisomers is given; the ortho/para (o/p) ratio was determined by ^{13}C NMR spectroscopy. [c]3.00 equiv. of allyltrimethylsilane and a reaction time of 36 h were used. [d]5.00 equivalents of benzeneselenol were used. Selected single-crystal x-ray structures are shown with the corresponding CCDC deposition numbers.

and (3) nucleophiles prone to Lewis-acid-induced polymerization or decomposition (e.g. thiophenes, furans, and alkenes). Thus, productive trapping requires a balance between nucleophilicity, Lewis basicity, and stability under the reaction conditions.

The [3.2]paracyclophane phenyl thioether **7a** was readily converted into the parent [3.2]paracyclophane hydrocarbon **16** by reductive desulfurisation using either Raney–Nickel/H_2 or $NaBH_4/NiCl_2{\cdot}6H_2O$ [42], giving the hydrocarbon in high yield (93% or 95%, respectively) (Scheme 4A). This transformation completes the formal [2.2]-to-[3.2] skeletal edit and provides a straightforward four-step access to the mixed-bridge [3.2] hydrocarbon framework from [2.2]paracyclophane (**1**). Furthermore, the whole sequence could be readily translated to the gram scale.

15213773, 0, Downloaded from https://onlinelibrary.wiley.com/doi/10.1002/anie.74911177 by Karlsruher Institut Fur Technologie, Wiley Online Library on [10/11/2026]. See the Terms and Conditions (https://onlinelibrary.wiley.com/terms-and-conditions) on Wiley Online Library for rules of use; OA articles are governed by the applicable Creative Commons License



SCHEME 4 | (A) Gram-scale formal skeletal editing of [2.2]paracyclophane to [3.2]paracyclophane. (B) Iterative bridge expansion. (C) Double bridge expansion. (D) Synthetic elaboration of [3.2]paracyclophane (**16**) toward thermally activated delayed fluorescence (TADF) emitter **28** (left), photoluminescence spectrum of the 10 wt% emitter-doped bis[2-(diphenylphosphino)phenyl]ether oxide (DPEPO) film (λ_{exc} = 360 nm, centre), and comparison of the photophysical properties with the corresponding ^{t}Bu[2.2]carbazolophane [45] emitter (right). A photograph of isolated **16** is shown in (A); single-crystal x-ray structures of **17** and the minor diastereomer of **22** are shown in (B) and (C), respectively. Abbreviations: r.r. = regioisomeric ratio and d.r. = diastereomeric ratio.

We next examined whether the phenonium-ion-mediated bridge expansion could be applied iteratively to an already expanded [3.2]paracyclophane (**16**) (Scheme 4B). Unlike the symmetric ethylene bridge of [2.2]paracyclophane (**1**), the three-carbon bridge of the [3.2]pCp hydrocarbon **16** offers two distinct positions for functionalization. Applying the chloroformylation–methanolysis/reduction sequence to this species regioselectively installed the hydroxymethyl group at the three-carbon bridge, as confirmed by single-crystal x-ray diffraction analysis of alcohol **17**. This selectivity is consistent with the more pronounced benzylic character of the functionalized position in the three-carbon bridge compared with the corresponding positions in the ethylene bridge. Subjecting alcohol **17** to the standard rearrangement conditions afforded the [4.2]paracyclophane thioether **18** in 91% isolated yield, and subsequent reductive desulfurization furnished the parent [4.2]paracyclophane (**19**) in 96% yield. Thus, the bridge-expansion sequence can be iteratively extended to higher-order paracyclophane topologies.

A bis-functionalised [2.2]paracyclophane substrate was prepared by chloroformylation of pCp ester **2**, followed by reduction of the resulting bisester (Scheme 4C). This sequence afforded alcohol **20** as a mixture of regio- and diastereomers, as confirmed by single-crystal x-ray diffraction analysis (see Section S3.11). Subjecting

15213773, 0, Downloaded from https://onlinelibrary.wiley.com/doi/10.1002/anie.74911177 by Karlsruher Institut Fur Technologie, Wiley Online Library on [10/11/2026]. See the Terms and Conditions (https://onlinelibrary.wiley.com/terms-and-conditions) on Wiley Online Library for rules of use; OA articles are governed by the applicable Creative Commons License

this mixture to the standard conditions led to efficient double bridge expansion, affording the corresponding [3.3]paracyclophane bis-thioether **22** as a mixture of diastereomers in 74% combined yield. The minor diastereomer could be selectively crystallized, and its structure was confirmed by x-ray diffraction. Subsequent reductive desulfurization of the diastereomeric bis-thioether mixture **22** then furnished the corresponding [3.3]paracyclophane hydrocarbon **23** in 92% yield.

Because bridge length in paracyclophanes directly affects molecular geometry, strain, interdeck distance, and transannular electronic communication, higher paracyclophane homologues represent attractive building blocks for functional molecular architectures [29, 30]. To demonstrate that the bridge-expanded scaffolds obtained by this methodology can be further elaborated, we investigated the functionalization of parent [3.2]paracyclophane (**16**) (Scheme 4D). Electrophilic bromination provided mono- or dibrominated [3.2]paracyclophanes (**24** or **25**), while in the monobromination, substitution occurred preferentially on the arene deck adjacent to the shorter ethylene bridge [30]. Building on our recent work on [2.2]carbazolophane-based TADF emitters [43–45], we used monobrominated [3.2]paracyclophane **24** as an entry point to a bridge-expanded carbazolophane donor. Buchwald–Hartwig coupling with 2-chloroaniline followed by oxidative cyclisation furnished donor **27**, which was subsequently coupled with 2-(4-fluorophenyl)-4,6-diphenyl-1,3,5-triazine (FPTZ) to give the donor–acceptor emitter **28**. Photophysical characterization in a 10 wt% doped film in DPEPO revealed sky-blue emission at λ_{PL} of 486 nm with a photoluminescence quantum yield, Φ_{PL}, of 97% under nitrogen (85% in air), representing a significant improvement over the corresponding [2.2]carbazolophane emitters [43–45]. Relative to the previously reported [2.2]^{t}BuCzp-Ph-TRZ benchmark [45], the bridge-expanded emitter exhibits slightly higher S_1 and T_1 levels, increasing from 2.87 to 2.93 eV for S_1 and from 2.69 to 2.81 eV for T_1, respectively, resulting in a reduced ΔE_{ST} of 0.12 versus 0.18 eV, although the delayed emission lifetime slightly increased from 315 to 352 µs, likely due to reduced non-radiative decay. Overall, these results demonstrate that bridge topology serves as an effective design parameter for cyclophane-based functional molecular architectures (see Section S3.12).

The unexpected tolerance of the reaction toward water suggested that the reaction warranted closer mechanistic examination. Accordingly, an in-situ ^{1}H NMR spectroscopy experiment was conducted to monitor the reaction kinetics (Scheme 5A). Interestingly, the starting-material and product profiles displayed an induction period and sigmoidal kinetics, suggesting a self-accelerating process (see Section S3.13) [46–48].

Since water is generated from the alcohol substrate and protic nucleophile during the reaction, we hypothesized that water-induced changes in BF_3 speciation could account for the observed self-acceleration. In particular, we considered the in-situ formation of $BF_3{\cdot}H_2O$, which is described in the literature as a Brønsted acid and for which rate-accelerating effects in BF_3-mediated reactions have been documented [49–55]. To test whether $BF_3{\cdot}H_2O$ is indeed formed under the reaction conditions, we conducted ^{11}B and ^{19}F NMR spectroscopy control experiments (Scheme 5B). Mixing the pCp alcohol **3** with $BF_3{\cdot}OEt_2$ gave a single ^{11}B resonance at $\delta_B = 0.05$ ppm. Addition of 0.35 equivalents of water generated a second signal at $\delta_B = -1.01$ ppm, which was also observed in a reaction mixture sampled after three hours. The ^{19}F NMR experiments gave analogous results. After water addition, a second ^{19}F resonance at $\delta_F = -150.5$ ppm appeared and the initial resonance shifted from $\delta_F = -152.6$ ppm to $\delta_F = -153.5$ ppm, with both signals reproduced in the sampled reaction mixture. Furthermore, in-situ ^{11}B and ^{19}F NMR spectroscopy experiments confirmed the gradual formation of this species during the reaction (see Section S3.13). Notably, Zhang reported ^{11}B NMR spectral shifts for $BF_3{\cdot}H_2O$ in very good agreement with our data, while excluding other boron species such as HBF_4 and H_3BO_3 [51]. Accordingly, based on our control experiments and the literature precedent, we assign the newly formed species to $BF_3{\cdot}H_2O$ and conclude that it forms progressively over the course of the reaction.

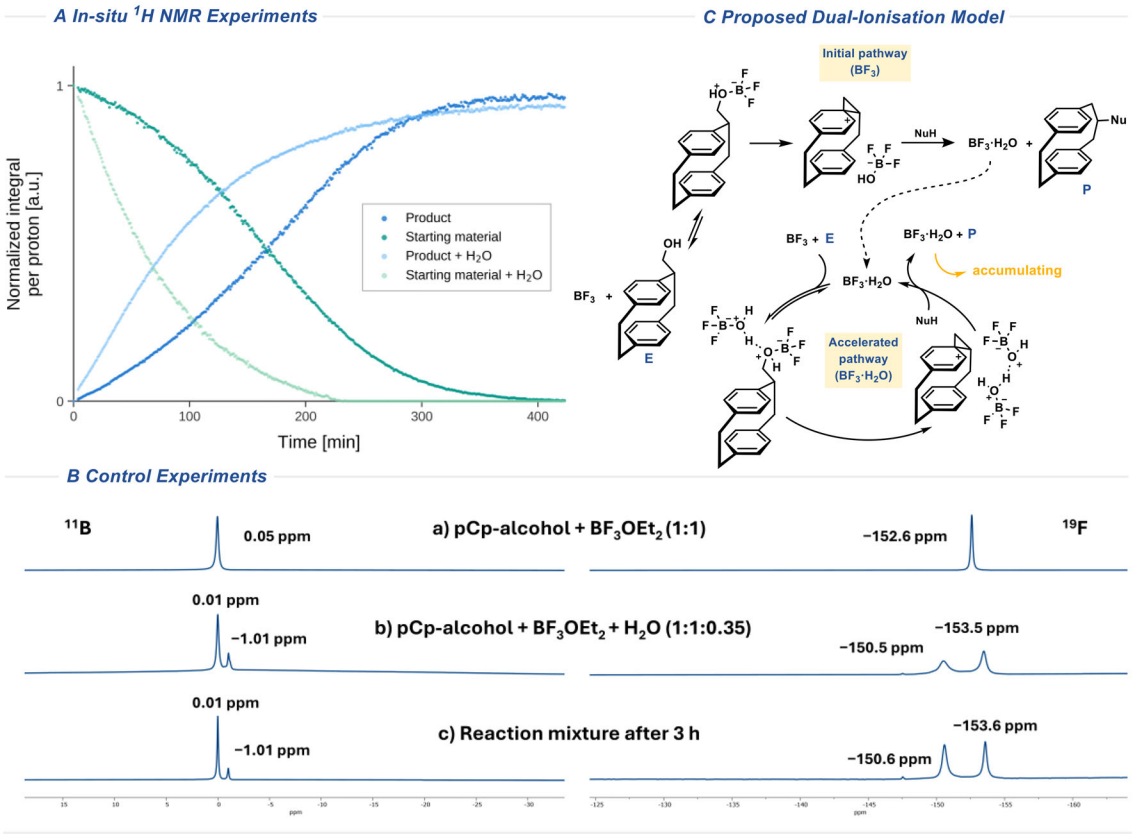
To determine whether the in-situ formation of $BF_3{\cdot}H_2O$ affects the kinetic profile, an additional ^{1}H NMR spectroscopy experiment was performed under otherwise identical conditions in the presence of 0.35 equivalents of added water (Scheme 5A). Compared with the original experiment, the induction period was effectively eliminated and both substrate consumption and product formation were accelerated. These findings strongly support the involvement of $BF_3{\cdot}H_2O$ in the observed self-acceleration.

Assuming ionization to be rate determining, the kinetic and control experiments support a dual-ionization model (Scheme 5C). Within this model, at the start of the reaction, $BF_3{\cdot}OEt_2$ promotes slow ionisation of the pCp alcohol **E**, generating small amounts of thioether product **P** and water. The water formed in this process shifts BF_3 speciation toward $BF_3{\cdot}H_2O$, which opens an alternative, lower-barrier pathway for phenonium-ion formation. Continued water release during product formation increases the concentration of $BF_3{\cdot}H_2O$, which, together with the lower ionisation barrier, accounts for the observed induction period and self-acceleration. This dual role of BF_3, acting both as an initial Lewis acid activator and as the precursor to the more active $BF_3{\cdot}H_2O$ species, may also rationalise the unique performance of $BF_3{\cdot}OEt_2$ observed during the optimisation studies.

To establish how $BF_3{\cdot}H_2O$ promotes ionization at the molecular level, we examined plausible pathways by density functional theory (DFT) calculations. The initial pathway involves Lewis-acid-mediated ionization, whereas we first interpreted the $BF_3{\cdot}H_2O$-enabled pathway as Brønsted-acid-mediated, in line with the literature precedent [51–55]. However, the results discussed below point to a more intricate chemical scenario.

As expected, the calculated Gibbs free-energy profile for the $BF_3{\cdot}OEt_2$-mediated pathway shows that ionization is energetically highly demanding, with **TS-I** located at $\Delta G^{\ddagger} = 29.0$ kcal mol^{-1} relative to the BF_3-activated pCp alcohol **I** (Scheme 6A). The transition geometry shows simultaneous elongation of the C—O bond and formation of the new C—C bond in a nearly collinear arrangement, consistent with the classical S_N2-type description of phenonium-ion formation, in which leaving-group departure and C—C bond formation occur in a concerted fashion [56]. Subsequent interception of the phenonium ion by thiophenol is nearly barrierless ($\Delta G^{\ddagger} = 2.1$ kcal mol^{-1}), and formation of the [3.2]pCp thioether **III** is strongly exergonic relative to **I** ($\Delta G = -19.4$ kcal mol^{-1}).

15213773, 0, Downloaded from https://onlinelibrary.wiley.com/doi/10.1002/anie.7491177 by Karlsruher Institut Fur Technologie, Wiley Online Library on [10/11/2026]. See the Terms and Conditions (https://onlinelibrary.wiley.com/terms-and-conditions) on Wiley Online Library for rules of use; OA articles are governed by the applicable Creative Commons License



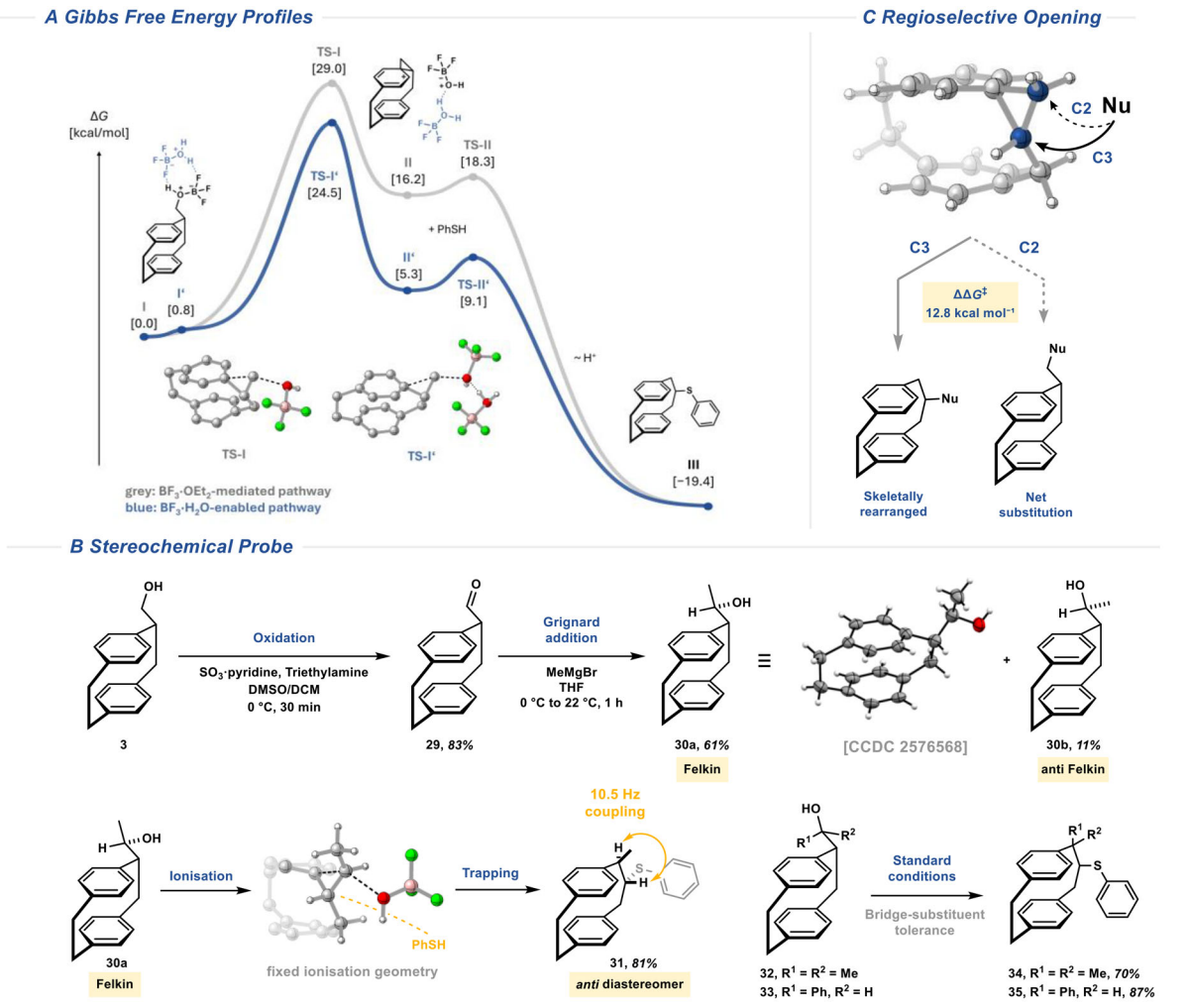
SCHEME 5 | (A) In-situ ^{1}H NMR spectroscopy experiment reveals sigmoidal kinetic profile. (B) ^{11}B and ^{19}F NMR control experiments for (a) pCp alcohol **3** and $BF_3{\cdot}OEt_2$, (b) after addition of H_2O, and (c) the reaction mixture after 3 h. (C) Proposed dual-ionization model.

Central to the proposed self-acceleration model is whether $BF_3{\cdot}H_2O$ enables a lower-energy pathway for phenonium-ion formation. Notably, all attempts to locate a stationary point corresponding to a discrete protonated pCp alcohol were unsuccessful. Although a concerted protonation–ionisation pathway was identified, its effective barrier of 29.1 kcal mol^{-1} is essentially identical to that of the $BF_3{\cdot}OEt_2$-mediated pathway (see Section S5.3). Taken together, these findings argue against a classical Brønsted-acid mechanism. Instead, the calculations revealed a cooperative $BF_3/BF_3{\cdot}H_2O$ pathway. In the reactant complex **I′**, $BF_3{\cdot}H_2O$ interacts through a cyclic pair of O—H···F hydrogen bonds with the BF_3-complex **I**. Upon formation of **TS-I′**, the alcohol oxygen accepts a hydrogen bond from $BF_3{\cdot}H_2O$ which facilitates C—O bond cleavage by stabilising the departing trifluoro(hydroxy)borate moiety. This cooperative activation lowers the effective ionisation barrier to 24.5 kcal mol^{-1}, 4.5 kcal mol^{-1} below that of the $BF_3{\cdot}OEt_2$-mediated pathway. The resulting phenonium intermediate **II′** is also substantially lower in free energy than **II** on the common reference scale ($\Delta\Delta G = -10.9$ kcal mol^{-1}). Thus, in our system, $BF_3{\cdot}H_2O$ is best understood not as a conventional Brønsted acid, but as a hydrogen-bond donor that facilitates leaving-group departure within a Lewis-acid-activated complex.

We next used the stereochemical behaviour of substituted alcohol substrates as an experimental probe (Scheme 6B). Oxidation of the alcohol **3** to the corresponding pCp aldehyde **29**, followed by diastereoselective addition of methylmagnesium bromide, furnished the Felkin alcohol **30a** as the major product together with the anti-Felkin alcohol **30b**. The relative configuration of the major diastereomer **30a** was assigned by single-crystal X-ray diffraction. Subjecting the Felkin alcohol **30a** to the standard rearrangement conditions afforded the corresponding [3.2]paracyclophane thioether **31** as a single *anti*-diastereomer. The *anti* relationship between the apical proton and the benzylic proton was established by coupling-constant analysis (see Section S3.14). This outcome is consistent with the calculated transition-state geometry and supports a stereospecific rearrangement. In contrast, the anti-Felkin alcohol **30b** decomposed under the same conditions, and the origin of this divergent behavior could not be conclusively established. Notably, this decomposition was not observed for other benzylic substituents: the corresponding bis-methyl alcohol **32** afforded rearranged product **34** in 70% yield, while mono-phenyl-substituted alcohol **33**, used as a mixture of diastereomers, afforded rearranged product **35** as a diastereomeric mixture in 87% yield (see Section S3.15).

A second key feature of the pCp-derived phenonium ion is its highly regioselective ring opening (Scheme 6C). Controlling regioselectivity is central for phenonium-ion-mediated transformations, and recent work by Race has made important progress in addressing this challenge through reagent-controlled ring opening [13]. In the present system, nucleophilic attack could in principle occur at either C2 or C3. While C2 attack would lead to net substitution, C3 attack gives the bridge-expanded framework. Calculations show that C3 attack is favoured over C2 attack by a substantial $\Delta\Delta G^{\ddagger}$ of 12.8 kcal mol^{-1}, accounting for

15213773, 0, Downloaded from https://onlinelibrary.wiley.com/doi/10.1002/anie.74911177 by Karlsruher Institut Fur Technologie, Wiley Online Library on [10/11/2026]. See the Terms and Conditions (https://onlinelibrary.wiley.com/terms-and-conditions) on Wiley Online Library for rules of use; OA articles are governed by the applicable Creative Commons License



SCHEME 6 | (A) Calculated Gibbs free-energy profiles for the $BF_3{\cdot}OEt_2$-mediated pathway (grey) and the $BF_3{\cdot}H_2O$-enabled pathway (blue). Calculations were performed at the SMD(1,2-dichloroethane)/ωB97X-D4/def2-TZVP//CPCM(1,2-dichloroethane)/ωB97X-D4/def2-TZVP level using Garza–Gellrich solution-entropy corrections [57, 58]. Relative Gibbs free energies are given in kcal mol^{-1} and referenced to I + $BF_3{\cdot}H_2O$ + PhSH. (B) Stereochemical probe supports stereospecific phenonium-ion formation and trapping. (C) Regioselectivity of phenonium-ion ring opening. Selected calculated geometries are shown in (A)–(C); the single-crystal x-ray structure of **30a** is shown in (B).

the highly regioselective, substrate-controlled outcome observed experimentally.

3 | Conclusion

In summary, this work establishes a modular phenonium-ion-mediated strategy for the skeletal editing of paracyclophanes. Synthetic control over the pCp-derived phenonium ion is achieved through direct alcohol activation under nonpolar conditions that avoid solvolysis, using the dual-role Lewis acid $BF_3{\cdot}OEt_2$ that initiates formation of the cationic intermediate and serves as the precursor for the in-situ formation of $BF_3{\cdot}H_2O$, which further promotes ionization. Under these conditions, external nucleophiles can outcompete self-trapping and oligomerization when present in sufficient concentration and compatible with the Lewis acidic medium. The intrinsic regioselectivity of the pCp-derived phenonium ion channels the reactivity toward bridge expansion rather than net substitution. Under operationally simple conditions, this strategy tolerates a diverse range of nucleophiles and provides modular access to [3.2]paracyclophanes. Reductive desulfurization delivers the parent hydrocarbons, and the sequence can be translated to gram scale, applied iteratively to higher homologues, and extended to double bridge expansion. The resulting higher paracyclophane topologies serve as functional building blocks, as exemplified by the incorporation into a TADF emitter architecture. Together, these results define pCp-derived phenonium ions as controllable intermediates for skeletal editing and provide a practical entry into higher paracyclophane homologues for synthesis and materials-oriented applications.

Author Contributions

Tilman Köhler: conceptualization, methodology, investigation, validation, formal analysis, data curation, visualization, project administration, writing – original draft, and writing – review and editing. **Pascal Marx:** investigation, validation. **André Jung:** investigation, validation, formal analysis, data curation, visualization, and writing – review and editing. **Maximilian Hartmann:** software, writing – review and editing.

15213773, 0, Downloaded from https://onlinelibrary.wiley.com/doi/10.1002/anie.74911177 by Karlsruher Institut Fur Technologie, Wiley Online Library on [10/11/2026]. See the Terms and Conditions (https://onlinelibrary.wiley.com/terms-and-conditions) on Wiley Online Library for rules of use; OA articles are governed by the applicable Creative Commons License

Jasmin Seibert: methodology, resources, writing – review and editing. **Olaf Fuhr:** investigation, formal analysis, data curation, validation, visualization, and writing – review and editing. **Eli Zysman-colman:** validation, resources, supervision, and writing – review and editing. **Stefan Bräse:** conceptualization, supervision, resources, project administration, funding acquisition, and writing – review and editing.

Acknowledgments

The authors thank Prof. Matthias Olzmann and Prof. Joachim Podlech for helpful discussions and Dr. Andreas Rapp for assistance with the analytical experiments. T. K. gratefully acknowledges financial support from the Fonds der Chemischen Industrie (FCI). Support from the Karlsruhe School of Optics & Photonics (KSOP) and the Ministry of Science, Research and the Arts of Baden–Württemberg within the framework of the sustainability funding of projects of the Excellence Initiative II is gratefully acknowledged. M. H. acknowledges funding from the German Research Foundation (Deutsche Forschungsgemeinschaft, DFG) through the Priority Programme SPP 2363 (project number 460865652). The authors also acknowledge support from the state of Baden–Württemberg through bwHPC. The UK team thanks the Engineering and Physical Sciences Research Council for support (EP/Z535291/1 and EP/W007517/1).

Open access funding enabled and organized by Projekt DEAL.

Conflicts of Interest

The authors declare no conflicts of Interest.

Data Availability Statement

The experimental and analytical data supporting the findings of this study are available in the Supporting Information and through the Chemotion Repository (https://www.chemotion-repository.net). Individual dataset DOIs are linked to the corresponding experiments in the Supporting Information, and the complete data collection is available at https://doi.org/10.14272/collection/TIK_2026-06-08 [59]. Additional research data associated with this study are available from the University of St Andrews Data Repository at https://doi.org/10.17630/171bbfde-db49-45af-8fe3-26cd2bfa1a01. Crystallographic data for compounds 7b, 11o, 12a–c, 13, 17, 20b, 22, and 30a have been deposited with the Cambridge Crystallographic Data Centre (CCDC) under deposition numbers 2576559–2576568. Computational details, calculated energies, and Cartesian coordinates are provided in the Supporting Information.

References

1. D. J. Cram, "Studies in Stereochemistry. I. The Stereospecific Wagner–Meerwein Rearrangement of the Isomers of 3-Phenyl-2-butanol," *Journal of the American Chemical Society* 71 (1949): 3863–3870, https://doi.org/10.1021/ja01180a001.

2. D. J. Cram, "Studies in Stereochemistry. III. The Wagner–Meerwein Rearrangement in the 2-Phenyl-3-pentanol and 3-Phenyl-2-pentanol Systems," *Journal of the American Chemical Society* 71 (1949): 3875–3883, https://doi.org/10.1021/ja01180a003.

3. D. J. Cram, "Studies in Stereochemistry. V. Phenonium Sulfonate Ion-Pairs as Intermediates in the Intramolecular Rearrangements and Solvolysis Reactions That Occur in the 3-Phenyl-2-Butanol System," *Journal of the American Chemical Society* 74 (1952): 2129–2137, https://doi.org/10.1021/ja01129a001.

4. G. A. Olah and R. D. Porter, "Stable Carbonium Ions. CXV. Ethylenephenonium and Ethylene-p-Toluonium Ions," *Journal of the American Chemical Society* 92 (1970): 7627–7629, https://doi.org/10.1021/ja00729a041.

5. G. A. Olah and R. D. Porter, "Stable Carbocations. CXXI. Carbon-13 Magnetic Resonance Spectroscopy Study of Ethylenarenium Ions (Spiro[2.5]Octadienyl Cations)," *Journal of the American Chemical Society* 93 (1971): 6877–6887, https://doi.org/10.1021/ja00754a031.

6. G. A. Olah, N. J. Head, G. Rasul, and G. K. S. Prakash, "Protonation of Benzocyclobutene With Superacid: Cram's Phenonium Ion (Spiro[5.2]octa-5,7-dien-4-yl Cation) Revisited," *Journal of the American Chemical Society* 117 (1995): 875–882, https://doi.org/10.1021/ja00108a003.

7. Y. Tsuji and J. P. Richard, "Formation and Mechanism for Reactions of Ring-Substituted Phenonium Ions in Aqueous Solution," *Journal of Physical Organic Chemistry* 29 (2016): 557–564, https://doi.org/10.1002/poc.3510.

8. R. J. Mayer and D. Lebœuf, "Harnessing Phenonium Ions in Synthesis," *Angewandte Chemie International Edition* 64 (2025): e202516932, https://doi.org/10.1002/anie.202516932.

9. S. M. Banik, J. W. Medley, and E. N. Jacobsen, "Catalytic, Asymmetric Difluorination of Alkenes to Generate Difluoromethylated Stereocenters," *Science* 353 (2016): 51–54, https://doi.org/10.1126/science.aaf8078.

10. F. Scheidt, J. Neufeld, M. Schäfer, C. Thiehoff, and R. Gilmour, "Catalytic *Geminal* Difluorination of Styrenes for the Construction of Fluorine-rich Bioisosteres," *Organic Letters* 20 (2018): 8073–8076, https://doi.org/10.1021/acs.orglett.8b03794.

11. F. Scheidt, M. Schäfer, J. C. Sarie, C. G. Daniliuc, J. J. Molloy, and R. Gilmour, "Enantioselective, Catalytic Vicinal Difluorination of Alkenes," *Angewandte Chemie International Edition* 57 (2018): 16431–16435, https://doi.org/10.1002/anie.201810328.

12. J. Li, A. Bauer, G. Di Mauro, and N. Maulide, "α-Arylation of Carbonyl Compounds Through Oxidative C−C Bond Activation," *Angewandte Chemie International Edition* 58 (2019): 9816–9819, https://doi.org/10.1002/anie.201904899.

13. S. Xu, H. M. Holst, S. B. McGuire, and N. J. Race, "Reagent Control Enables Selective and Regiodivergent Opening of Unsymmetrical Phenonium Ions," *Journal of the American Chemical Society* 142 (2020): 8090–8096, https://doi.org/10.1021/jacs.0c02095.

14. S. Zhang, M. Vayer, F. Noël, et al., "Unlocking the Friedel-Crafts Arylation of Primary Aliphatic Alcohols and Epoxides Driven by Hexafluoroisopropanol," *Chem* 7 (2021): 3425–3441, https://doi.org/10.1016/j.chempr.2021.10.023.

15. M. Van Hoof, R. J. Mayer, J. Moran, and D. Lebœuf, "Triflic Acid-Catalyzed Dehydrative Amination of 2-Arylethanols With Weak N -Nucleophiles in Hexafluoroisopropanol," *Angewandte Chemie International Edition* 64 (2025): e202417089, https://doi.org/10.1002/anie.202417089.

16. L. Ruyet, C. Roblick, J. Häfliger, et al., "Catalytic Ring Expanding Difluorination: An Enantioselective Platform to Access β,β-Difluorinated Carbocycles," *Angewandte Chemie International Edition* 63 (2024): e202403957, https://doi.org/10.1002/anie.202403957.

17. X. Lei, Y. Li, Y. Lai, et al., "Strain-Driven Dyotropic Rearrangement: A Unified Ring-Expansion Approach to α-Methylene-γ-Butyrolactones," *Angewandte Chemie International Edition* 60 (2021): 4221–4230, https://doi.org/10.1002/anie.202013169.

18. H. Hopf, in *Modern Cyclophane Chemistry* (Wiley-VCH, 2004).

19. H. Hopf, "[2.2]Paracyclophanes in Polymer Chemistry and Materials Science," *Angewandte Chemie International Edition* 47 (2008): 9808–9812, https://doi.org/10.1002/anie.200800969.

20. J. Paradies, "[2.2]Paracyclophane Derivatives: Synthesis and Application in Catalysis," *Synthesis* 2011 (2011): 3749–3766, https://doi.org/10.1055/s-0031-1289296.

21. Z. Hassan, E. Spuling, D. M. Knoll, J. Lahann, and S. Bräse, "Planar Chiral [2.2]Paracyclophanes: From Synthetic Curiosity to Applications in Asymmetric Synthesis and Materials," *Chemical Society Reviews* 47 (2018): 6947–6963, https://doi.org/10.1039/C7CS00803A.

22. H. Tappert and S. Bräse, "[2.2]Paracyclophane Materials—Status and Perspectives," *Macromolecular Rapid Communications* 46 (2025): 2500145, https://doi.org/10.1002/marc.202500145.

23. T. Köhler, M. Hartmann, O. Fuhr, and S. Bräse, "Planar Chirality Controls Diastereotopicity in [2.2]Paracyclophanyl Cyclopropenes,"

15213773, 0, Downloaded from https://onlinelibrary.wiley.com/doi/10.1002/anie.74911177 by Karlsruher Institut Fur Technologie, Wiley Online Library on [10/11/2026]. See the Terms and Conditions (https://onlinelibrary.wiley.com/terms-and-conditions) on Wiley Online Library for rules of use; OA articles are governed by the applicable Creative Commons License

Chemistry—A European Journal 32 (2026): e70876, https://doi.org/10.1002/chem.70876.

24. Z. Hassan, E. Spuling, D. M. Knoll, and S. Bräse, "Regioselective Functionalization of [2.2]Paracyclophanes: Recent Synthetic Progress and Perspectives," *Angewandte Chemie International Edition* 59 (2020): 2156–2170, https://doi.org/10.1002/anie.201904863.

25. R. Sun, T. Ye, L. Micouin, and E. Benedetti, "Unlocking the Functionalization and Reactivity of Ethylene Bridges in [2.2]Paracyclophanes: Strategies and Challenges," *European Journal of Organic Chemistry* 29 (2026): e70505, https://doi.org/10.1002/ejoc.70505.

26. X. Zhang, Y. Zhou, Z.-X. Yu, C.-H. Tung, and Z. Xu, "Strained Dehydro-[2,2]-Paracyclophane Enabled Planar Chirality Construction and [2.2]Paracyclophane Functionalization," *Angewandte Chemie International Edition* 64 (2025): e202420667, https://doi.org/10.1002/anie.202420667.

27. D. Ly, J. Bacsa, and H. M. L. Davies, "Rhodium(II)-Catalyzed Asymmetric Cyclopropanation and Desymmetrization of [2.2]Paracyclophanes," *ACS Catalysis* 14 (2024): 6423–6431, https://doi.org/10.1021/acscatal.4c01292.

28. D. Chen, Y. Zhou, C.-H. Tung, Z.-X. Yu, and Z. Xu, "A Desymmetric Dearomatization Cyclopropanation of [2.2]Paracyclophane," *CCS Chemistry* 7 (2025): 1509–1521, https://doi.org/10.31635/ccschem.024.202404067.

29. Z. Pechlivanidis, H. Hopf, and L. Ernst, "Paracyclophanes: Extending the Bridges. Synthesis," *European Journal of Organic Chemistry* 2009 (2009): 223–237, https://doi.org/10.1002/ejoc.200800494.

30. Z. Pechlivanidis, H. Hopf, J. Grunenberg, and L. Ernst, "Paracyclophanes: Extending the Bridges. Reactions," *European Journal of Organic Chemistry* 2009 (2009): 238–252, https://doi.org/10.1002/ejoc.200800748.

31. S. Misumi and T. Otsubo, "Chemistry of Multilayered Cyclophanes," *Accounts of Chemical Research* 11 (1978): 251–256, https://doi.org/10.1021/ar50126a005.

32. V. G. Haensch, H. Görls, and C. Hertweck, "A Photochemical Macrocyclization Route to Asymmetric Strained [3.2] Paracyclophanes," *Chemistry—A European Journal* 28 (2022): e202202577, https://doi.org/10.1002/chem.202202577.

33. T. Köhler, O. Fuhr, and S. Bräse, "[2.2]Paracyclophane-Substituted Quinolines by Skeletal Editing Strategies," *Organic Chemistry Frontiers* 12 (2025): 3546–3550, https://doi.org/10.1039/D5QO00505A.

34. D. J. Cram and F. L. Harris, "Macro Rings. XXXV. Stereochemistry of [2.2]Paracyclophanyl Nucleus as a Neighboring Group in Solvolyses Reactions," *Journal of the American Chemical Society* 89 (1967): 4642–4651, https://doi.org/10.1021/ja00994a014.

35. D. J. Cram and R. E. Singler, "Stereochemistry. XLII. Highly Strained Phenonium Ion Incorporated in the [2.2]Paracyclophane System," *Journal of the American Chemical Society* 93 (1971): 4443–4450, https://doi.org/10.1021/ja00747a018.

36. E. Hedaya and L. M. Kyle, "The Fate of the 1-([2.2]Paracyclophanyl)Methylcarbonium Ion. A Double-Barrelled Ring Expansion Route to the [3.3]Paracyclophane System," *Journal of the American Chemical Society* 88 (1966): 3667–3669, https://doi.org/10.1021/ja00967a050.

37. J. Nishimura, Y. Okada, and A. Oku, "Phenonium Ion in [3.n]Paracyclophanes. Effects of Neighboring Groups, Steric Size of Substituents, and Strain on Solvolysis Reactions," *The Journal of Organic Chemistry* 51 (1986): 1838–1843, https://doi.org/10.1021/jo00360a034.

38. M. S. Kharasch, S. S. Kane, and H. C. Brown, "Carboxylation. III. The Peroxide-Catalyzed Reaction of Oxalyl Chloride With the Side-Chains of Aralkyl Hydrocarbons. A Preliminary Study of the Relative Reactivity of Free Radicals," *Journal of the American Chemical Society* 64 (1942): 1621–1624, https://doi.org/10.1021/ja01259a041.

39. E. Hedaya and L. M. Kyle, "Bridge Chemistry of Paracyclophanes. The Mono- and Dichloroformylation of [2.2]Paracyclophane (Di-p-Xylylene) With Oxalyl Chloride," *Journal of Organic Chemistry* 32 (1967): 197–199, https://doi.org/10.1021/jo01277a047.

40. M. Brookhart, F. A. L. Anet, D. J. Cram, and S. Winstein, "Phenonium and Benzylic Cations From 3-Phenyl-2-butanols in FSO_3 H-SbF^l," *Journal of the American Chemical Society* 88 (1966): 5659–5660, https://doi.org/10.1021/ja00975a060.

41. L. Pitzer, F. Schäfers, and F. Glorius, "Rapid Assessment of the Reaction-Condition-Based Sensitivity of Chemical Transformations," *Angewandte Chemie International Edition* 58 (2019): 8572–8576, https://doi.org/10.1002/anie.201901935.

42. J. Rentner, M. Kljajic, L. Offner, and R. Breinbauer, "Recent Advances and Applications of Reductive Desulfurization in Organic Synthesis," *Tetrahedron* 70 (2014): 8983–9027, https://doi.org/10.1016/j.tet.2014.06.104.

43. N. Sharma, E. Spuling, C. M. Mattern, et al., "Turn on of Sky-blue Thermally Activated Delayed Fluorescence and Circularly Polarized Luminescence (CPL) *via* Increased Torsion by a Bulky Carbazolophane Donor," *Chemical Science* 10 (2019): 6689–6696, https://doi.org/10.1039/c9sc01821b.

44. A. K. Gupta, Z. Zhang, E. Spuling, et al., "Electron-Withdrawing Group Modified Carbazolophane Donors for Deep Blue Thermally Activated Delayed Fluorescence OLEDs," *Materials Advances* 2 (2021): 6684–6693, https://doi.org/10.1039/d1ma00738f.

45. J. Seibert, Y. Xu, H. Hafeez, et al., "A Novel Carbazolophane: A Comparison of the Performance of Two Planar Chiral CP-TADF Emitters," *Advanced Functional Materials* 34 (2024): 2401956, https://doi.org/10.1002/adfm.202401956.

46. A. J. Bissette and S. P. Fletcher, "Mechanisms of Autocatalysis," *Angewandte Chemie International Edition* 52 (2013): 12800–12826, https://doi.org/10.1002/anie.201303822.

47. M. Dryzhakov and J. Moran, "Autocatalytic Friedel–Crafts Reactions of Tertiary Aliphatic Fluorides Initiated by $B(C_6 F_5)_3 \cdot H_2 O$," *ACS Catalysis* 6 (2016): 3670–3673, https://doi.org/10.1021/acscatal.6b00866.

48. J. Kaur and J. P. Barham, "Shedding Light on Synthetic Autocatalysis: From Conventional Closed-Shell Chemistries to Overlooked Open-Shell Occurrences," *Chemistry—A European Journal* 32 (2026): e02075, https://doi.org/10.1002/chem.202502075.

49. A. M. Eastham, "Co-Catalysis in Friedel-Crafts Reactions. I. Boron Fluoride-Water," *Journal of the American Chemical Society* 78 (1956): 6040–6042, https://doi.org/10.1021/ja01604a024.

50. J. M. Clayton and A. M. Eastham, "Cocatalysis in Friedel-Crafts Reactions. II. Boron Fluoride-Water," *Journal of the American Chemical Society* 79 (1957): 5368–5369, https://doi.org/10.1021/ja01577a008.

51. S. Zhang, X. Zhang, X. Ling, et al., "Superacid $BF_3 - H_2 O$ Promoted Benzylation of Arenes With Benzyl Alcohols and Acetates Initiated by Trace Water," *RSC Advances* 4 (2014): 30768–30774, https://doi.org/10.1039/C4RA04059G.

52. R. Huang, X. Zhang, J. Pan, et al., "Benzylation of Arenes With Benzyl Halides Synergistically Promoted by In Situ Generated Superacid Boron Trifluoride Monohydrate and Tetrahaloboric Acid," *Tetrahedron* 71 (2015): 1540–1546, https://doi.org/10.1016/j.tet.2015.01.037.

53. M. Huang, L. Hu, H. Shen, et al., "Sulfination of Alcohols With Sodium Sulfinates Promoted by BF 3 ·OEt 2 : An Unexpected Access," 18 (2016): 1874–1879, https://doi.org/10.1039/C5GC02846A.

54. P. Singh and R. K. Peddinti, "In Situ Generated Superacid BF_3–H_2O Catalyzed Alkylation of p-Quinols With Diaryl Carbinols Leading to Triarylmethanes," *Journal of Chemical Sciences* 134 (2022): 63, https://doi.org/10.1007/s12039-022-02054-0.

55. S.-W. Yu, Z.-J. Chen, Z.-H. Chen, et al., "Trace Water in a $BF_3 \cdot OEt_2$ System: A Facile Access to Sulfinyl Alkenylsulfones From Alkynes and Sodium Sulfinates," *Organic & Biomolecular Chemistry* 21 (2023): 7776–7781, https://doi.org/10.1039/D3OB01249B.

15213773, 0, Downloaded from https://onlinelibrary.wiley.com/doi/10.1002/anie.74911177 by Karlsruher Institut Fur Technologie, Wiley Online Library on [10/11/2026]. See the Terms and Conditions (https://onlinelibrary.wiley.com/terms-and-conditions) on Wiley Online Library for rules of use; OA articles are governed by the applicable Creative Commons License

56. H. M. Holst, S. B. McGuire, and N. J. Race, "Revisiting the 'Phenonium Phenomenon': Regiodivergent Opening of Nonsymmetrical Phenonium Ions With Halide Nucleophiles," *Synlett* 32 (2021): 01–06, https://doi.org/10.1055/s-0040-1706420.

57. A. J. Garza, "Solvation Entropy Made Simple," *Journal of Chemical Theory and Computation* 15 (2019): 3204–3214, https://doi.org/10.1021/acs.jctc.9b00214.

58. J. Ariai and U. Gellrich, "The Entropic Penalty for Associative Reactions and Their Physical Treatment During Routine Computations," *Physical Chemistry Chemical Physics* 25 (2023): 14005–14015, https://doi.org/10.1039/d3cp00970j.

59. T. Köhler, "Chemotion Repository," (2026), https://doi.org/10.14272/collection/TIK_2026-06-08.

60. Chemotion Repository, https://www.chemotion-repository.net.

61. P.-C. Huang, C.-L. Lin, P. Tremouilhac, N. Jung, and S. Bräse, "Using the Chemotion Repository to Deposit and Access FAIR Research Data for Chemistry Experiments," *Nature Protocols* 20 (2025): 1097–1098, https://doi.org/10.1038/s41596-024-01074-z.

62. D. Kelly, L. G. Franca, K. Stavrou, A. Danos, and A. P. Monkman, "Laplace Transform Fitting as a Tool To Uncover Distributions of Reverse Intersystem Crossing Rates in TADF Systems," *Journal of Physical Chemistry Letters* 13 (2022): 6981–6986, https://doi.org/10.1021/acs.jpclett.2c01864.

63. D. Fărcaşiu and M. Stan, "Strength of Lewis Acid–Lewis Base Interactions. A 13C NMR Study of the Ether Interchange in Boron Trifluoride Complexes," *Journal of the Chemical Society, Perkin Transactions* 2 (1998): 1219–1222, https://doi.org/10.1039/A709073K.

64. O. V. Dolomanov, L. J. Bourhis, R. J. Gildea, J. A. K. Howard, and H. Puschmann, "*OLEX2* : A Complete Structure Solution, Refinement and Analysis Program," *Journal of Applied Crystallography* 42 (2009): 339–341, https://doi.org/10.1107/S0021889808042726.

65. G. M. Sheldrick, "*SHELXT*—Integrated Space-group and Crystal-Structure Determination," *Acta Crystallographica Section A: Foundations and Advances* 71 (2015): 3–8, https://doi.org/10.1107/S2053273314026370.

66. G. M. Sheldrick, "Crystal Structure Refinement With SHELXL," *Acta Crystallographica Section C: Structural Chemistry* 71 (2015): 3–8, https://doi.org/10.1107/S2053229614024218.

67. F. Neese, "The ORCA Program System," *WIREs Computational Molecular Science* 2 (2012): 73–78, https://doi.org/10.1002/wcms.81.

68. F. Neese, "Software Update: The ORCA Program System—Version 6.0," *Wiley Interdisciplinary Reviews: Computational Molecular Science* 15 (2025): e70019, https://doi.org/10.1002/wcms.70019.

69. M. Hartmann, F. Schönle, J. Wagner, et al., "DELFIN: Automated DFT-Based Prediction of Preferred Spin States and Corresponding Redox Potentials," *ChemRxiv* (2025), https://doi.org/10.26434/chemrxiv-2025-4c256.

70. G. Landrum, P. Tosco, B. Kelley, et al., "rdkit/rdkit: 2026_03_3 (Q1 2026) Release," *Zenodo* (2026), https://doi.org/10.5281/zenodo.20446949.

71. B. de Souza, "GOAT: A Global Optimization Algorithm for Molecules and Atomic Clusters," *Angewandte Chemie International Edition* 64 (2025): e202500393, https://doi.org/10.1002/anie.202500393.

72. C. Bannwarth, S. Ehlert, and S. Grimme, "GFN2-xTB—An Accurate and Broadly Parametrized Self-Consistent Tight-Binding Quantum Chemical Method With Multipole Electrostatics and Density-Dependent Dispersion Contributions," *Journal of Chemical Theory and Computation* 15 (2019): 1652–1671, https://doi.org/10.1021/acs.jctc.8b01176.

73. N. Mardirossian and M. Head-Gordon, "ωB97X-V: A 10-parameter, Range-separated Hybrid, Generalized Gradient Approximation Density Functional With Nonlocal Correlation, Designed by a Survival-of-the-fittest Strategy," *Physical Chemistry Chemical Physics* 16 (2014): 9904, https://doi.org/10.1039/C3CP54374A.

74. A. Najibi and L. Goerigk, "DFT -D4 Counterparts of Leading Meta-Generalized-Gradient Approximation and Hybrid Density Functionals for Energetics and Geometries," *Journal of Computational Chemistry* 41 (2020): 2562–2572, https://doi.org/10.1002/jcc.26411.

75. E. Caldeweyher, C. Bannwarth, and S. Grimme, "Extension of the D3 Dispersion Coefficient Model," *Journal of Chemical Physics* 147 (2017): 034112, https://doi.org/10.1063/1.4993215.

76. E. Caldeweyher, S. Ehlert, A. Hansen, et al., "A Generally Applicable Atomic-Charge Dependent London Dispersion Correction," *Journal of Chemical Physics* 150 (2019): 154122, https://doi.org/10.1063/1.5090222.

77. F. Weigend and R. Ahlrichs, "Balanced Basis Sets of Split Valence, Triple Zeta Valence and Quadruple Zeta Valence Quality for H to Rn: Design and Assessment of Accuracy," *Physical Chemistry Chemical Physics* 7 (2005): 3297, https://doi.org/10.1039/B508541A.

78. F. Neese, F. Wennmohs, A. Hansen, and U. Becker, "Efficient, Approximate and Parallel Hartree–Fock and Hybrid DFT Calculations. A 'Chain-of-Spheres' algorithm for the Hartree–Fock Exchange," *Chemical Physics* 356 (2009): 98–109, https://doi.org/10.1016/j.chemphys.2008.10.036.

79. R. Izsák and F. Neese, "An Overlap Fitted Chain of Spheres Exchange Method," *Journal of Chemical Physics* 135 (2011): 144105, https://doi.org/10.1063/1.3646921.

80. F. Weigend, "Accurate Coulomb-Fitting Basis Sets for H to Rn," *Physical Chemistry Chemical Physics* 8 (2006): 1057, https://doi.org/10.1039/B515623H.

81. V. Barone and M. Cossi, "Quantum Calculation of Molecular Energies and Energy Gradients in Solution by a Conductor Solvent Model," *Journal of Physical Chemistry A* 102 (1998): 1995–2001, https://doi.org/10.1021/jp9716997.

82. M. Garcia-Ratés and F. Neese, "Effect of the Solute Cavity on the Solvation Energy and Its Derivatives Within the Framework of the Gaussian Charge Scheme," *Journal of Computational Chemistry* 41 (2020): 922–939, https://doi.org/10.1002/jcc.26139.

83. A. V. Marenich, C. J. Cramer, and D. G. Truhlar, "Universal Solvation Model Based on Solute Electron Density and on a Continuum Model of the Solvent Defined by the Bulk Dielectric Constant and Atomic Surface Tensions," *Journal of Physical Chemistry B* 113 (2009): 6378–6396, https://doi.org/10.1021/jp810292n.

84. G. A. Crosby and J. N. Demas, "Measurement of Photoluminescence Quantum Yields. Review," *Journal of Physical Chemistry* 75 (1971): 991–1024, https://doi.org/10.1021/j100678a001.

85. W. H. Melhuish, "Quantum Efficiencies of Fluorescence of Organic Substances: Effect of Solvent and Concentration of the Fluorescent Solute[1]," *Journal of Physical Chemistry* 65 (1961): 229–235, https://doi.org/10.1021/j100820a009.

Supporting Information

Additional supporting information can be found online in the Supporting Information section.

The authors have cited additional references within the Supporting Information [59–85].

Supporting File: anie75512-sup-0001-SuppMat.docx.

15213773, 0, Downloaded from https://onlinelibrary.wiley.com/doi/10.1002/anie.74911177 by Karlsruher Institut Fur Technologie, Wiley Online Library on [10/11/2026]. See the Terms and Conditions (https://onlinelibrary.wiley.com/terms-and-conditions) on Wiley Online Library for rules of use; OA articles are governed by the applicable Creative Commons License